

Chandra Observations and Optical Identification of Hard X-ray Sources Discovered with ASCA

Shin WATANABE^{1,2} Masayuki AKIYAMA³ Yoshihiro UEDA¹

Kouji OHTA⁴ Richard MUSHOTZKY⁵ Tadayuki TAKAHASHI^{1,2} and Toru YAMADA⁶

¹*Institute Space and Astronautical Science, Sagamihara, Kanagawa, 229-8510*

²*Department of Physics, University of Tokyo, Tokyo, 113-0033*

³*Subaru Telescope, National Astronomical Observatory of Japan, Hilo, HI, 96720, USA*

⁴*Department of Astronomy, Kyoto University, Kyoto, 606-8502*

⁵*NASA Goddard Space Flight Center, Greenbelt, Maryland, 20771, USA*

⁶*National Astronomical Observatory of Japan, Mitaka, Tokyo, 181-8588*

watanabe@astro.isas.ac.jp

(Received 2002 June 25; accepted 2002 August 12)

Abstract

We present the first results of the Chandra and optical follow-up observations of hard X-ray sources detected in the ASCA Medium Sensitivity Survey (AMSS). Optical identifications are made for five objects. Three of them show either weak or absent optical narrow emission lines and are at low redshift $\langle z \rangle \sim 0.06$. One of them is a broad line object at $z = 0.910$ and one is a $z = 0.460$ object with only narrow lines. All the narrow line objects show strong evidence for absorption in their X-ray spectra. Their line ratios are consistent with a Seyfert II/LINER identification as are the line widths. The three low redshift objects have the colors of normal galaxies and apparently the light is dominated by stars. This could be due to the extinction of the underlying nuclear continuum by the same matter that absorbs X-rays and/or due to the dilution of the central source by starlight. These results suggest that X-ray sources that appear as “normal” galaxies in optical and near-IR bands significantly contribute to the hard X-ray background. This population of objects has a high space density and probably dominates the entire population of active galaxies.

Key words: galaxies: active — surveys — X-rays: galaxies — X-rays: general

1. Introduction

The origin of the Cosmic X-ray Background (CXB) has been one of great mysteries in X-ray astronomy. At soft X-ray energies (below 2 keV), the ROSAT surveys resolved 70–80 % of the CXB into discrete sources (e.g., Hasinger et al. 1998). The majority of the

optical identifications are unobscured active galactic nuclei (AGNs), mostly Seyfert Is and quasars (Lehmann et al. 2001). At higher energies, an additional population of absorbed or flat spectrum objects are needed to make up the CXB, which has a flatter spectrum in the 2–10 keV band than the unobscured AGNs.

Hard X-ray surveys performed with ASCA resolved about 30 % of the CXB in the 2–10 keV band, revealing the presence of a population of hard sources emerging at flux levels of several 10^{-13} erg cm $^{-2}$ s $^{-1}$ (Ueda et al. 1999a; Ueda et al. 1999b). Recently, almost all of the hard X-ray background has been resolved into point sources by the Chandra deep surveys (e.g., Mushotzky et al. 2000; Brandt et al. 2000; Giacconi et al. 2001). The faint sources detected with Chandra have, on average, rather hard spectra (e.g., Rosati et al. 2002), which indeed account for the spectrum of the CXB. However, due to the faintness of the Chandra sources in the optical band, their nature still remains, in general unclear (Barger et al. 2001).

In order to understand this hard X-ray population over a broad range in luminosity and redshift, it is necessary to reveal the nature of the “bright” sources (i.e., with fluxes above 10^{-13} erg cm $^{-2}$ s $^{-1}$ in the 2–10 keV band) that make up about 30 % of the CXB. In addition, because of their brightness, these sources should be much easier to study over a wide range of wavelengths than the ultra-faint Chandra sources, and serve as a prototype of the key populations that comprise the CXB. The results of the optical identification of a complete hard-band selected sample in the ASCA Large Sky Survey (ALSS, Akiyama et al. 2000) indicates that the majority of the hard sources are nearby ($z \lesssim 0.5$) type-2 AGNs. However, in particular when sources with hard X-ray spectra are concerned, our knowledge is still quite limited due to the small sample size.

Thus, we have started to study the optical counterparts of the “bright” and “hard” sources selected from the ASCA Medium Sensitivity Survey (AMSS; Ueda et al. 2001), a serendipitous source survey of the extragalactic sky based on the ASCA GIS archival data at flux limits of 10^{-13} erg cm $^{-2}$ s $^{-1}$ (2–10 keV). The advantage of the AMSS is its large solid angle of sky coverage, which is indispensable for obtaining a reasonable sample of “bright” (hence rare) sources.

In this paper we report the first results of the Chandra observations and optical identifications for hard AMSS sources selected in Chandra AO-1. The excellent positional accuracy of ~ 1 arcsec obtained with Chandra has enabled us to make unambiguous optical identifications of these sources. We present the results from X-ray, optical, and near infrared observations, in § 2, 3 and 4, respectively, followed by detailed description of individual sources in § 5. We discuss the results in § 5 and our conclusions are given in § 6. Throughout the paper, we assume a Hubble constant of $H_0 = 50$ km s $^{-1}$ Mpc $^{-1}$ and a deceleration parameter of $q_0 = 0.5$. Optical identification for a complete flux-limited sample using a part of the AMSS catalog is reported by Akiyama et al. (2002).

2. X-ray Data

2.1. The Sample

Table 1 lists the seven sources that were selected for Chandra AO1 observations. We selected them from an AMSS catalog with the following two criteria¹ : (1) Objects are detected in the 2–10 keV band with a flux fainter than 3×10^{-13} erg cm⁻² s⁻¹ (assuming a photon index of 1.7), but (2) not detected in the 0.7–2 keV band, with detection significance above 4.5σ . None of the sources have ROSAT HRI or PSPC counterparts when the ROSAT image is available, and the best-fit photon index in the ASCA data is less than 0.8, consistent with or flatter than the X-ray background spectral slope within the error. Because this sample is selected essentially without any bias, they are considered to be a good representative of the X-ray population with hard X-ray spectra at fluxes of $(1-3) \times 10^{-13}$ erg cm⁻² s⁻¹ (2–10 keV). We selected these sources from an earlier version of the AMSS catalog than the published one (Ueda et al. 2001). Also, we adopted a slightly lower threshold for detection significance (4.5σ) than that used for the published catalog (5.0σ). As a result, some sources in this sample do not exist in the catalog published by Ueda et al. (2001). The corresponding source names of the AMSS catalog (with a prefix of “1AXG”), if present, are listed in Table 1. None of them are in the sample of Akiyama et al. (2002), who use slightly brighter sources with more conservative detection criteria. The total number of 2–10 keV detected ($\geq 5\sigma$) sources at Galactic latitudes $|b| > 20^\circ$ that have similar properties (i.e., with the apparent photon index smaller than 0.8 at the flux range of $(1-3) \times 10^{-13}$ erg cm⁻² s⁻¹) is 18 out of about 800 serendipitous sources in the Ueda et al. (2001) catalog.

2.2. Chandra Results

The log of Chandra observations is given in Table 1. All the observations were performed with the ACIS detector (Bautz et al. 1998), placing the target near the aim point of the ACIS-I array on the CCD I3 chip. We analyzed the data in a standard manner using the “CIAO 2.1” software. We performed source search by the “*celldetect*” program, which uses a simple sliding cell method. From all the seven fields, we detected X-ray sources in the ASCA error circle. We found, however, that the results for two of the targets are rather different than expected from the ASCA results. The Chandra 2–10 keV flux of AXJ 1227+4421 (10^{-14} erg cm⁻² s⁻¹) is more than ten times less than the ASCA flux. Similarly, in the error circle of AXJ 2018+1139, two X-ray sources were detected with fluxes of 10^{-14} erg cm⁻² s⁻¹, whose summed flux does not account for the ASCA-measured flux. Possible reasons for the discrepancy are discussed in § 5.1. In this paper, we concentrate on the other five sources that have clear Chandra

¹ In the subsequent Chandra AO2 and AO3 observations we select targets with slightly different criteria and strategy from the published AMSS catalog, both aiming at somewhat brighter sources with fluxes above 3×10^{-13} erg cm⁻² s⁻¹ (2–10 keV). The details will be given in future papers.

counterparts for which optical identification was made.

Table 2 gives the X-ray properties of the five targets. The positions are accurate within $< 1''$. For reference we list “apparent” power-law photon indices from the hardness ratio $(H - S)/(H + S)$, where H and S is the count rate in the 2–10 keV and 0.7–2 keV bands, respectively, correcting for the Galactic absorption.

Fig. 1 shows the ACIS pulse height spectra. Using the redshift determined from the optical identification (see § 3), we calculated the amounts of absorption at the source redshift assuming a photon index fixed at 1.7, a typical value for AGNs (e.g., Mushotzky et al. 1993). Because the background is negligible and the number of photons in each bin is very small, we used the Poisson likelihood statistics to search for the best-fit parameters and the errors. We find that the column densities for AXJ 0223+421, AXJ 0431–0526, AXJ 1025+4714 and AXJ 1510+0742 are $N_{\text{H}} \sim 10^{22-23} \text{ cm}^{-2}$, and that for AXJ 1951+5609 is $\sim 10^{21} \text{ cm}^{-2}$. Using the best-fit parameters, we calculate the observed 2–10 keV flux and the absorption-corrected 2–10 keV luminosity. These results are also summarized in Table 2. The range of X-ray luminosity is $\sim 10^{41-45} \text{ erg s}^{-1}$.

Since AXJ 1025+4714 has sufficient photon counts, we fit its spectrum with both the photon index and column density being free parameters. Fig. 2 shows the confidence contour for the two parameters. This indicates that the hard spectrum cannot be attributed purely to an intrinsically flat spectrum and a significant amount of absorption is indeed required.

3. Optical Data

3.1. Observations

We conducted optical follow-up observations for the five Chandra sources corresponding to AXJ 0223+4212, AXJ 0431–0526, AXJ 1025+4714, AXJ 1510+0742, and AXJ 1951+5609. Firstly, optical counterparts of the Chandra sources are selected from the Digitized Palomar Observatory Sky Survey plate (hereafter DPOSS). All the five sources have only one optical counterpart above the limit of the DPOSS. Based on the range of optical to X-ray fluxes one anticipates that, as opposed to the fainter Chandra and XMM sources, the optical counterparts of the ASCA sources are expected to be in the 15–18th mag range, well above the flux limits of the DPOSS (see Figure 3 of Hasinger et al. (1999), which shows the observed range of X-ray to optical fluxes.) and thus their detection in the DPOSS images is expected. Spectroscopic observations of the optical counterparts were made during the course of optical follow-up observations for a complete hard-band selected sample of the AMSS (Akiyama et al. 2002). A detailed journal of observation of each source is shown in Table 3.

For AXJ 0223+4212, AXJ 0431–0526, AXJ 1025+4714, and AXJ 1510+0742, spectroscopic observations with the University of Hawaii 88” telescope were obtained on 5, 6 October

² Chandra science center memo http://cxc.harvard.edu/mta/ASPECT/celmon/index_update.html

2000, and 20, 21 March 2001, respectively. We used the Wide Field Grism Spectrograph with a grating of 420 grooves mm^{-1} and the blaze wavelength of 6400 Å. The spatial resolution was 0."35 pixel^{-1} and the typical image size during the observations was 0."8 – 1."2. A slit width of 1."2 was used. We covered the wavelength range from 4000 Å to 8000 Å without an order cut filter. The spectral resolution, which was measured by the HgAr lines in comparison frames and night-sky lines in object frames, was 12 Å (FWHM) which corresponds to 500 km s^{-1} at 7000 Å. We took imaging data of each object without any filter with higher spatial resolution than the DPOSS. Fig. 3 shows the no-filter 60" \times 60" images of the four sources.

For AXJ 1951+5609, the spectroscopic observation was done at the KPNO 2.1 m telescope on 20 September 2000. We used the Gold Camera Spectrograph with Grating (#32) with 300 grooves mm^{-1} and blaze wavelength of 6750 Å. The spatial sampling was 0."78 pixel^{-1} . The typical image size during the observation was 2."0. The slit width was 2."0 for objects and 10 " for standard star observations. The dispersion was 2.47 Å pixel^{-1} . We covered the wavelength range from 4000 Å to 8000 Å with an order cut filter for the wavelength range shorter than 4000 Å (GG400). The spectral resolution was measured to be 8 Å (FWHM) from night-sky lines in object frames.

3.2. Analysis and Results

All of the data were analyzed using IRAF³. After bias subtraction, flat-fielding, and wavelength calibration, optimum extraction method with the "apeextract" package was used to extract one dimensional spectral data from the two dimensional original data. Flux calibration of the one dimensional spectral data was made with spectra of standard stars (Feige 34 and BD+28 are standard stars for March and October runs, respectively). The finding chart made from the DPOSS and the flux calibrated optical spectrum of each object are shown in Fig. 4. Basic parameters of the sample are listed in Table 4.

Based on flux-calibrated spectrum of each object, we estimated the magnitude of the objects. The flux density at 6400 Å of each object is converted to the *R*-band magnitude. The estimated *R*-band magnitudes are listed in Table 4. Because the slit aperture of the spectroscopic observation does not cover the whole area of the objects, the magnitudes represent those in that region. The uncertainty of the estimation of the magnitude is ± 0.9 magnitude without the slit-aperture loss.

While all of the optical counterparts show emission lines, only AXJ 1951+5609 shows a strong broad emission line. To evaluate the strength and the velocity width of the narrow emission lines of the other four sources quantitatively, we performed spectral fitting for the lines using a χ^2 minimization method with the "specfit" command in the "spfitpkg" package

³ IRAF is distributed by the National Optical Astronomy Observatories, which is operated by the Association of Universities for Research in Astronomy, Inc. (AURA) under cooperative agreement with the National Science Foundation.

of IRAF. The FWHMs of line widths were deconvolved by the spectral resolution mentioned above and are given in Table 5. Measured flux ratios of the [OIII] λ 5007 to H β the [NII] λ 6583 to H α , and the [SII] $\lambda\lambda$ 6717, 6731 to H α are also listed in Table 5, and are plotted in Fig. 5. Solid lines in the figure represent boundaries between Seyfert II galaxies, LINERs, and H II region-like galaxies taken from Veilleux and Osterbrock 1987 and Veilleux 1995.

4. Near-Infrared Data

AXJ 0223+4212, AXJ 0431–0526, and AXJ 1025+4714 are detected in the 2MASS survey⁴ and their J , H , and K_s band magnitudes are summarized in Table 6. For AXJ 1510+0742 and AXJ 1951+5609, we conducted near-infrared photometric observation with the SQUID (Simultaneous Quad Infrared Imaging Device) infrared camera with four 512 \times 512 ALADDIN InSb arrays attached to Kitt Peak National Observatory 2.1 m telescope on 31 March 2002. J -, H -, K_s -, and L -band images were taken simultaneously but here we use only J -, H -, and K_s -band data. The pixel scale of the camera was 0."69 pixel⁻¹. The FWHM of point sources during the observation was 1."3, 1."4, and 1."5, in the J -, H -, and K_s -bands, respectively. In each band, five frames each of which consists of 18 (for AXJ 1510+0742) or 12 (for AXJ 1951+5609) coaddition of 10s integration were taken, thus in total, the effective integrations were 900 s and 600 s for AXJ 1510+0742 and AXJ 1951+5609, respectively. The pixel scale of the camera was 0."69 pixel⁻¹. The seeing condition during the observation was 1."3, 1."4, and 1."5, in the J -, H -, and K_s -bands. During the observation, UKIRT faint standard stars (FS11, FS16, FS17, FS21, FS23, FS27) were observed for photometric calibration. For each star, we took 5 images with 5 coaddition of 10 s integration, changing the position of the star on the detector to reduce any systematic errors.

The data reduction were done in the following steps. At first, we subtracted a dark frame, which is made from a stacking of 10 images of a cold shutter with the same integration time, from the object data. The dark-subtracted frames were flat-fielded with a flat image, which is made by stacking the object frames with normalizing their background level. Finally, after correcting the offset of each object frame, we combined 5 frames of the each object. Dark-subtraction and flat-fielding were done for standard star frames in the same manner, but we did not shift and combine the standard star frames. Counts of the standard star in each frame were measured individually by using a growth curve fitting method for each star. Based on the scatter of the count rate to magnitude conversion factors derived from the observed UKIRT faint standard stars, we estimated the uncertainties of the photometric calibration as 0.02 mag, 0.04 mag, and 0.02 mag in J -, H -, and K_s -bands, respectively. The measured magnitudes of AXJ 1510+0742 and AXJ 1951+5609 were summarized in Table 6. The uncertainties include not only the scatter in the conversion factors but also the uncertainties caused by sky background determination in

⁴ <http://www.ipac.caltech.edu/2mass/>

the final object frame.

5. Detailed Description on Individual Sources

This section summarizes the optical, near infrared, and hard X-ray properties of each object in our sample. As already mentioned, only narrow ($v < 1000 \text{ km}^{-1}$) emission lines are detected in the optical spectra except for AXJ 1951+5609.

AXJ 0223+4212 ($z = 0.0435$, filled square in Figs. 5, 6, and 7): Narrow emission lines of $\text{H}\beta$, $\text{H}\alpha$, $[\text{NII}]\lambda\lambda 6548, 6583$, and $[\text{SII}]\lambda\lambda 6717, 6731$ are detected. $[\text{OIII}]\lambda 5007$ is not detected. The upper limit on the $[\text{OIII}]\lambda 5007$ to $\text{H}\beta$ flux ratio, the large $[\text{NII}]\lambda 6583$ to $\text{H}\alpha$ flux ratio, and the large $[\text{SII}]\lambda\lambda 6717, 6731$ to $\text{H}\alpha$ flux ratio are consistent with the line ratios of LINERs (Fig. 5). The narrow emission lines are not resolved. The estimated 2–10 keV luminosity is $3 \times 10^{41} \text{ erg s}^{-1}$ from the Chandra flux. This is the lowest luminosity object in this sample and its luminosity is similar to the lowest luminosity objects found in deep Chandra surveys and the very lowest luminosity Seyfert I galaxies. The optical image of the object shows two spiral arms and the object is classified as late-type spiral (Sb) galaxy.

AXJ 0431–0526 ($z = 0.0596$, filled circle): Narrow emission lines of $[\text{OIII}]\lambda\lambda 4959, 5007$, $\text{H}\alpha$, $[\text{NII}]\lambda\lambda 6548, 6583$, and $[\text{SII}]\lambda\lambda 6717, 6731$ are detected. $\text{H}\beta$ emission is not detected. The lower limit on the $[\text{OIII}]\lambda 5007$ to $\text{H}\beta$ flux ratio, the large $[\text{NII}]\lambda 6583$ to $\text{H}\alpha$ flux ratio, and the large $[\text{SII}]\lambda\lambda 6717, 6731$ to $\text{H}\alpha$ flux ratio are consistent with the line ratios of Seyfert IIs (Fig. 5). The narrow emission lines are not resolved and with an upper limit of $< 500 \text{ km s}^{-1}$ are only consistent with the narrowest line widths found in Seyfert IIs. The optical image shows the object is an early type galaxy (E or S0).

AXJ 1025+4714 ($z = 0.0617$, filled hexagon): Narrow emission lines of $\text{H}\beta$, $[\text{OIII}]\lambda\lambda 4959, 5007$, $\text{H}\alpha$, $[\text{NII}]\lambda\lambda 6548, 6583$, and $[\text{SII}]\lambda\lambda 6717, 6731$ are detected. The intermediate $[\text{OIII}]\lambda 5007$ to $\text{H}\beta$ flux ratio, the large $[\text{NII}]\lambda 6583$ to $\text{H}\alpha$ flux ratio, and the large $[\text{SII}]\lambda\lambda 6717, 6731$ to $\text{H}\alpha$ flux ratio fall in the region of Seyfert IIs but are also consistent with LINERs within the error (Fig. 5). The narrow emission lines are not resolved. In the blue side of the $\text{H}\alpha$ emission line, there is a hint (4σ) of a broad emission line with velocity width of $(3100 \pm 600 \text{ km s}^{-1})$ (compare $[\text{NII}]\lambda 6548 + \text{H}\alpha$ profile of the object with those of AXJ 0223+4212 and AXJ 0431–0526, see Fig. 4). The X-ray luminosity is more than an order of magnitude larger than that of typical LINERs ($\lesssim 10^{42} \text{ erg s}^{-1}$, Terashima et al. 2002). This implies that the object is more like a Seyfert II rather than a LINER. The host galaxy is E or S0.

AXJ 1510+0742 ($z = 0.4595$, filled triangle): Narrow emission lines of $[\text{OII}]\lambda 3727$ and $[\text{OIII}]\lambda\lambda 4959, 5007$ are detected. The presence of an $\text{H}\beta$ emission line is rather marginal; the significance of the line is about 2.5σ due to the dip features seen at the both side of the emission-like feature. Thus the lower limit on $[\text{OIII}]\lambda 5007/\text{H}\beta$ seems to be close to the true

value. The $[\text{OIII}]\lambda 5007/\text{H}\beta$ ratio implies that the emission lines originate from star-forming regions presumably with low-metallicity or Seyfert/LINER nucleus. The $\text{H}\alpha$ - $[\text{NII}]\lambda\lambda 6548, 6583$ wavelength range is not covered, and thus we could not distinguish between either a Seyfert II/LINER or a low-metallicity star-forming galaxy from the line ratio analysis. The $[\text{OIII}]\lambda 5007$ emission line is resolved, and the velocity width is estimated to be $500 \pm 50 \text{ km s}^{-1}$, typical of the velocity width of narrow $[\text{OIII}]\lambda 5007$ emission lines seen in Seyfert galaxies (Whittle 1992) and much larger than those of dwarf star-forming galaxies. In addition, the absolute magnitude of ~ -22 mag also supports the Seyfert II/LINER interpretation. Finally the large X-ray luminosity ($2 \times 10^{44} \text{ erg s}^{-1}$) suggests that the object is a (high luminosity) AGN rather than a LINER. The optical image is slightly ($< 1''$) extended.

AXJ 1951+5609 ($z = 0.910$, filled diamond): The object show broad MgII $\lambda 2800$ emission line with velocity width of $5800 \pm 500 \text{ km s}^{-1}$. The object-frame equivalent width of the broad MgII $\lambda 2800$ line is $60_{-20}^{+40} \text{ \AA}$ consistent with those of optically-selected QSOs ($50 \pm 29 \text{ \AA}$; Francis et al. 1991). The near-infrared ($J - Ks = 1.24$) and optical-to-near-infrared ($R - Ks = 2.5$) colors of this object are also consistent with the colors of optically-selected QSOs at redshift around 1. The X-ray luminosity of $7 \times 10^{44} \text{ erg s}^{-1}$ is the largest in our sample. The Chandra spectrum is apparently harder than a canonical power law photon index of 1.7 and the presence of absorption of $\lesssim 10^{22} \text{ cm}^{-2}$ is suggested, although its significance is marginal within the statistics of our data.

6. Discussion

6.1. X-ray Time Variability

Two out of the seven ASCA sources observed by Chandra are at least ten times weaker than seen in the ASCA data. To check if this is attributable to selection effects in the ASCA data and/or the result of source confusion, we re-examined the results of Monte Carlo simulations as performed in § 3 of Ueda et al. (2001). With the same selection criteria for significance (above 4.5σ in the 2–10 keV band and below 4.5σ in the 0.7–2 keV band) and flux ($< 3 \times 10^{-13} \text{ erg cm}^{-2} \text{ s}^{-1}$ in the 2–10 keV band) as for the present sample, we find that the probability that the flux measured with the ASCA GIS is more than 10 times larger than the real flux to be 6%, assuming that 20% of sources in the sky are highly absorbed at these flux levels (Akiyama et al. 2000). Hence, the expected number of false detections in our sample is 0.4. Note that the requirement of “no detection in the soft band” works to increase the fraction of false detections in the sample if the majority of sources have non-absorbed spectra, because unlike non-absorbed sources, the statistical fluctuation is independent of the energy bands. Given the areal density of Chandra sources at a flux level of $10^{-14} \text{ erg cm}^{-2} \text{ s}^{-1}$ of $\sim 200 \text{ deg}^{-2}$ the probability that an unrelated source will fall in the $\sim 1 \text{ arcmin}^2$ AMSS error circle is only

0.05. Thus it is unlikely that these Chandra sources are completely unrelated to the AMSS objects.

Thus, it is likely that these objects truly have a large variability range, although we do not rule out the possibility that either of the two is not real. Besides the two sources, AXJ 0223+4212 also shows a similar amplitude of variability. While detailed variability studies on times scales of years are only available for the brightest 25 AGNs, it is not unusual for objects to vary by factors of five over time scales of years and factors of ten are not unknown (e.g., Peterson et al. (2000) for NGC4051 and Weaver (1996) for NGC2992). Thus it is not clear if the pattern of variability of these objects is unusual. However the large amplitude of variability confirms that these objects are indeed AGNs.

6.2. Summary of Identification and Comparison with Other Surveys

Here we summarize the results of identification for the five Chandra sources. Three show either weak or absent optical narrow emission lines and are at very low redshifts of $\langle z \rangle \sim 0.06$ (AXJ 0223+4212, AXJ 0431–0526, AXJ 1025+4714), one is a narrow line object at $z = 0.460$ (AXJ 1510+0742), and the other is a broad line object at $z = 0.910$ (AXJ 1951+5609). The optical line ratios, line widths, and the X-ray luminosity of the four narrow line objects indicate that they are consistent with their identifications as Seyfert II or LINER. Their X-ray spectra show strong evidence for high column densities.

The hard X-ray flux (f_X) and optical magnitudes (f_R) of the identified objects are plotted in Fig. 6. In the same figure, we plot hard X-ray selected AGNs from HEAO1-A2 (triangles), the AMSS (circles), the ALSS (squares), and Chandra Deep Field North (asterisks and crosses, crosses means upper limit on the optical magnitude). Note that the HELLAS sample (La Franca et al. 2002) falls on a similar range to the whole AMSS sample (see Akiyama et al. 2002). As seen from the figure, there is a wide variety of the f_X/f_R ratio in our sample: AXJ 1510+0742 and AXJ 1951+5609 have hard X-ray to optical flux ratio close to that of the optically-faint X-ray sources seen by Chandra and XMM ($\log f_X/f_R \gtrsim +1$), while the three low redshift sources show a much smaller ratio ($\log f_X/f_R < 0$). We defer to a later paper a detailed discussion of the origin of the wide range in the X-ray to optical flux ratios.

Fig. 7 the redshift versus apparent photon index plot of our sample together with the ALSS sample, a flux limited complete sample at similar flux levels (Akiyama et al. 2000). As seen in this figure, three sources in our Chandra sample are even harder than the hardest X-ray source in the ALSS (AXJ 131501+314) in terms of the best-fit photon index. For comparison, Table 7 summarizes the optical and X-ray properties of the five “hardest” sources in the above ALSS sample. These ALSS hard sources are all located at low redshifts of $z < 0.4$ and are identified as four narrow line AGNs and one broad line AGN (AXJ 130926+2952). Equivalent widths of a narrow emission line of H_α and $[OIII]\lambda 5007$ are also given in Table 7 (for line ratios see Table 3 of Akiyama et al. 2000). Except for AXJ 130926+2952, which shows a strong

[OIII] λ 5007 line, their equivalent widths are similar to those of the three nearby sources in our Chandra sample. Similar to the Chandra sample (see next section) most of the ALSS hard sources have the morphology of elliptical or early type spiral galaxies and no clear nucleus is visible in the optical images.

6.3. Hard X-ray Population of “Normal” Galaxies

In this subsection, we discuss the nature of the three nearby sources in our AMSS-Chandra sample (AXJ 0223+4212, AXJ 0431–0526, and AXJ 1025+4714), which are identified as Seyfert IIs or a LINERs. As we describe below, in many respects these sources are apparently “normal” galaxies, and could be considered to represent the major population of very hard sources at fluxes of 10^{-13} erg cm $^{-2}$ s $^{-1}$ (2–10 keV). They are all in the nearby universe with an average redshift of 0.06 and have a very low hard X-ray to optical flux ratio ($\log f_X/f_R < 0$). As shown in Fig. 3, these objects are clearly resolved and show no signs of a luminous nucleus. Interestingly, as opposed to virtually all optically selected Seyfert IIs, 80% of which are Sa or later in the sample of Ho et al. (1997) and McLeod & Rieke (1995), the host galaxies of AXJ 0431–0526 and AXJ 1025+4714 have the morphology of E or S0. This may be related to the fact that these X-ray selected sources have larger luminosities compared with the optically selected Seyfert IIs.

They all have similar $J - K$ colors, consistent with that of old elliptical galaxies at $z \sim 0.05$ ($J - K = 1$), and bluer than optically-selected QSOs at $z \lesssim 0.2$ ($J - K = 1.5 - 2$; Elvis et al. 1994). Additionally, the existence of NaD and Mgb absorption lines in the optical continuum spectra of the objects suggests that their continuum in the optical wavelength is dominated by emission from host galaxy. The X-ray to K -band flux ratio and the X-ray to optical flux ratio of these objects are smaller than normal QSOs. Even if the nuclei of AXJ 0223+4212, AXJ 0431–0526, and AXJ 1025+4714 are not affected by optical extinction (have similar f_X/f_R or f_X/f_K ratio to normal QSOs), the host galaxy components of these objects are brighter than the expected optical flux from the nucleus and may explain the relative weakness of the optical emission lines and the absence of a blue continuum by dilution of the nuclear component in the beam by starlight.

The optical line widths and equivalent widths themselves do not distinguish these objects from normal (i.e., non-AGN) galaxies. The upper limits of ~ 500 km s $^{-1}$ on the line widths are consistent with the distribution of line widths in Seyfert II galaxies (Figure 4 of Koski 1978) which has a average value of 600 km s $^{-1}$ with a 250 km s $^{-1}$ variance (see also Whittle (1992) who shows that OIII is a bit narrower with a median value of 325 km s $^{-1}$ with a variance of 200 km s $^{-1}$) and thus is not definitive in the classification of the objects. The low equivalent width of the lines and the fact that their intensity is similar to that found in a field galaxy sample (Tresse et al. 1999, Carter et al. 2001) again does not distinguish these objects. Similarly the luminosity of the lines is consistent with that seen in field galaxy samples. On the

other hand, as we have shown above, the line ratios of two objects lie in the ionization range seen for many Seyfert IIs and thus are indicative of AGN, and one has line ratios indicative of LINER activity. Such objects have been already detected in optical spectroscopic surveys of field galaxies: Carter et al. (2001) find $\sim 15\%$ of all field galaxies have "AGN-like" emission line ratios.

The colors of the three nearby objects are completely consistent with that of stars with no sign of a non-thermal continuum. However, these galaxies are optically luminous with $M_V \sim -(21-22)$ and the relatively low luminosity active nuclei in these objects may be hidden by the glare of the starlight despite the low redshifts. Using the Elvis et al. (1994) spectral energy distribution one predicts that the effective optical magnitude of the active nucleus would be $\sim 17-19$ mag assuming that the nucleus is not absorbed and thus rather difficult to detect from ground based observations. The fact that these rather bright nearby galaxies harbor "optically invisible" AGN shows the incompleteness of optical active galaxy searches. Since the colors of these objects also show no abnormalities they would be missed by color selected surveys like the Sloan digital sky survey. It is also possible that the nuclei are absorbed in the optical and UV bands by the same matter that absorbs the X-ray continuum, reducing the observed optical flux. The effective reddening corresponding to the X-ray column densities of $(0.5-15) \times 10^{22} \text{ cm}^{-2}$ is $A_V \sim 2-70$ mags thus effectively eliminating the optical-UV flux.

6.4. *Contribution to the X-ray background*

Our results indicate that "very hard" X-ray sources at fluxes of $\sim 10^{-13} \text{ erg cm}^{-2} \text{ s}^{-1}$ (2–10 keV) are mostly nearby $z < 0.5$ sources with a column density of $\sim 10^{22-23} \text{ cm}^{-2}$, rather than high redshift (hence high luminosity) objects with a higher column density of $\sim 10^{23-24} \text{ cm}^{-2}$. This fully supports the result of the ALSS and is a strong constraint on the unified models of the X-ray background. According to the calculation of Comastri et al. (2001) and Gilli et al. (2001), about half of sources with a column density $> 10^{22} \text{ cm}^{-2}$ should have redshifts greater than 1 at a flux of $\sim 1 \times 10^{-13} \text{ erg cm}^{-2} \text{ s}^{-1}$. We have to remember, however, that there could be bias against high redshift objects having moderate column densities in our Chandra sample because our selection criteria were based on the "apparent" hardness: due to K-correction absorbed sources at higher redshifts show softer spectra in the observer frame. Precise measurement of the column densities of slightly less hard sources detected in the ALSS and AMSS (Akiyama et al. 2002) is important for a definitive test of the unified model.

The optical counterparts of the hard, faint ASCA sources discussed in this paper have rather different properties from those of soft X-ray and optically selected AGN in the sense that they have earlier morphological types, do not possess a luminous optical or IR nucleus, have near-infrared colors similar to that of normal galaxies, and show only weak narrow emission lines. These unusual properties have already been seen in the ALSS hard sample (Table 7) and in the HELLAS survey at a similar X-ray flux level (Maiolino et al. 2000) as well as in the deeper

Chandra fields (e.g., Barger et al. 2001).

7. Summary

We present the results of the first third of our Chandra follow-up of faint hard X-ray selected ASCA sources. We have optical counterparts for five of the seven objects, since two of them were too faint to uniquely associate the Chandra with the ASCA source. Of these five optical counterparts three of them show either weak or absent optical lines of low physical and equivalent width and are at low redshift $\langle z \rangle \sim 0.06$. One of them is a $z = 0.460$ object with only narrow lines and one is a broad line object at $z = 0.910$. All the narrow line objects show strong evidence for absorption in their X-ray spectra, and their line ratios are consistent with a Seyfert II/LINER identification as are the line widths. The three nearby objects have the colors of normal galaxies and apparently the light is dominated by stars. This could be due to the extinction of the underlying nuclear continuum by the same matter that absorbs the X-rays and/or due to the dilution of the central source by starlight. These results suggest that X-ray sources that appear as “normal” galaxies in optical and near-IR bands with weak (but AGN-like) narrow emission lines significantly contribute to the hard X-ray background, supporting the previous results of the ALSS and the HELLAS. This population of objects has a high space density and probably dominates the entire population of active galaxies.

References

- Akiyama, M., Ohta, K., Yamada, T., Kashikawa, N., Yagi, M., Kawasaki, W., Sakano, M., Tsuru, et al., 2000 ApJ, 532, 700
- Akiyama, M. et al. in preparation (2002)
- Barger, A. J., Cowie, L. L., Mushotzky, R. F., Richards, E. A. 2001, AJ, 121, 662
- Barger, A.J., Cowie, L.L., Brandt, W.N., Capak, P., Garmire, G.P., Hornschemeier, A.E., Steffen, A.T., Wehner, E.H. 2002, astro-ph/0206370
- Bautz, M., 1998, Proc. SPIE, 3444, 210
- Brandt, W.N., Hornschemeier, A.E., Garmire, G.P., Schneider, D.P., Barger, A.J., Bautz, M.W., Burrows, D.N., Chartas, G., et al., 2000, AAS, 196, 3416
- Brandt, W.N., Alexander, D.M., Hornschemeier, A.E., Garmire, G.P., Schneider, D.P., Barger, A.J., Bauer, F.E., Broos, P.S., et al. 2001, AJ, 122, 2810
- Carter, B.J., Fabricant, D.G, Geller, M.J., Kurtz, M.J., McLean, B. 2001, ApJ, 559, 606
- Comastri, A., Fiore, F., Vignali, C., Matt, G., Perola, G.C., La Franca, F. 2001, MNRAS, 327, 781
- Elvis, M., Wilkes, B.J., McDowell, J.C. Green, R.F., Bechtold, J., Willner, S.P., Oey, M.S., Polonski, E., Cutri, R. 1994, ApJS, 95, 1
- Francis, P.J., Hewett, P.C., Foltz C.B., Chaffee, F.H., Weymann, R.J., Morris, S.L. 1991, ApJ, 373, 465
- Giacconi, R., Rosati, P., Tozzi, P., Nonimo, M., Hasinger, G., Norman, C., Bergeron, J., Borgani, S.,

et al., 2001 ApJ, 551, 624

Gilli, R., Salvati, M., Hasinger, G. 2001, A&A, 386, 407

Gotthelf, E.V., Ueda, Y., Fujimoto, R., Kii, T., Yamaoka, K., 2000, ApJ, 543, 417

Hasinger, G., Burg, R., Giacconi, R., Schmidt, M. Trüemper, J., Zamorani, G., 1998, A&A, 329, 482

Hasinger, G., Lehmann, I., Giacconi, R., Schmidt, M., Trüemper, J., Zamorani, G., 1999, astro-ph, 9901103

Ho, L.C., Filippenko, A.V., and Sargent, W.L.W. 1997, ApJ, 487, 568

Joguet, B., Kunth, D., Melnick, J., Terlevich, R., Terlevich, E 2001, A&A, 380, 19

Koski, A.T. 1978, ApJ, 223, 56

La Franca, F., Fiore F., Vignali, C., Antonelli, A., Comastri, A., Giommi, P., Matt, G., Molendi, S., et al., 2002, ApJ, 570, 100

Lehmann, I., Hasinger, G., Schmidt, M., Giacconi, R., Trüper, J., Zamorani, G., Gunn, J. E., Pozzetti, L., et al., 2001, A&A, 371, 833L

Maiolino, R., et al. 2000, A&A, 355, 47

McLeod , K.K., & Rieke, G.H. 1995, ApJ, 441, 96

Mushotzky, R., Done, C., Pounds, K.A., 1993, ARA&A, 31,717

Mushotzky, R.F., Cowie, L.L., Barger, A.J., Arnoud, K.A., 2000, Nature, 404, 459

Peterson, B. M. et al., 2000, ApJ, 542, 161

Piccinotti, G., Mushotzky, R.F., Boldt, E.A., Holt, S.S., Marshall, F.E., Serlemitsos, P.J., Shafer, R.A. 1982, ApJ, 253, 485

Rosati, P., et al. 2002, ApJ, 566, 667

Terashima, Y., Iyomoto, N., Ho, L.C., Ptak, A.F. 2002, ApJS, 139, 1

Tresse, L., Maddox, S., Loveday, J., Singleton, C. 1999, MNRAS, 310, 262

Ueda, Y., Takahashi, T., Inoue, H., Tsuru, T., Sakano, M., Ishisaki, Y., Ogasaka, Y., Makishima, K., et al., 1999a, ApJ, 518, 656

Ueda, Y., Takahashi, T., Ishisaki, Y., Ohashi, T., Makishima, K. 1999b, ApJ, 524, L11

Ueda, Y., Ishisaki, Y., Takahashi, T., Makishima, K., Ohashi, T. 2001, ApJS, 133, 1

Veilleux, S., Osterbrock, D.E. 1987, ApJS, 69, 295

Veilleux, S., 1995, ApJS, 98, 171

Weaver, K.A. et al., 1996, ApJ, 458, 160

Whittle, M. 1992, ApJS, 79, 49

Table 1. Target list of our observations with Chandra. The corresponding source name in the AMSS catalog (Ueda et al. 2001), if present, is given in the parenthesis. The position and flux are determined with ASCA. The ASCA error radius is 1–1.5 arcmin.

Target(Cataloged Name)	RA, DEC	ASCA flux*		Chandra Observation	
	(J2000)	2–10 keV	0.7–2 keV	Exposure	Date
AXJ 0223+4212(1AXG J022353+4212)	35.9719, 42.2083	3.0	0.21	6.48 ks	05 Sep. 2000
AXJ 0431–0526	67.9280, –5.4365	2.7	<0.06 [†]	5.97 ks	03 Oct. 2000
AXJ 1025+4714(1AXG J102557+4713)	156.4883, 47.2316	2.2	<0.08 [†]	4.77 ks	07 Jun. 2000
AXJ 1227+4421	186.9139, 44.3541	1.5	0.25	7.31 ks	04 Oct. 2000
AXJ 1510+0742	227.5974, 7.7006	2.5	<0.37 [†]	6.46 ks	01 Jun. 2000
AXJ 1951+5609(1AXG J195105+5610)	297.7717, 56.1677	2.0	0.37	8.47 ks	25 Apr. 2000
AXJ 2018+1139(1AXG J201822+1139)	304.5932, 11.6562	1.7	0.15	8.52 ks	30 Aug. 2000

*: in units of 10^{-13} erg cm⁻² s⁻¹. The flux is calculated from the best-fit count rate in the same band assuming a photon index of 1.7. Note that all the detection significance in the soft band (0.7–2 keV) is below 4.5 σ .

†: 1 σ upper limit.

Table 2. X-ray data of five Chandra sources that are clearly associated with the ASCA sources. Photon Indices are calculated from the hardness ratio between the 2–10 keV and 0.7–2 keV counts, correcting for Galactic absorption. The column density (at the source redshift) is determined assuming a photon index of 1.7. The flux is an observed one (i.e., not corrected for absorption nor for redshift), while the luminosity is corrected for absorption and is given in the 2–10 keV source frame, both calculated from the best-fit absorbed power-law model with a photon index of 1.7.

Target	RA, DEC (J2000)	Cts/ks 0.7–2 keV	Cts/ks 2–10 keV	Photon Index*	N _H [†] [10 ²² cm ⁻²]	Flux [erg cm ⁻² s ⁻¹]	Luminosity [erg s ⁻¹]
AXJ 0223+4212	35.9737, 42.2061	0.46	0.77	0.3±0.7	3.1 ^{+3.6} _{-2.1}	4.0 × 10 ⁻¹⁴	2.5 × 10 ⁴¹
AXJ 0431–0526	67.9134, –5.4320	0.34	8.9	–1.2±0.1	14.4 ^{+6.1} _{-5.1}	7.1 × 10 ⁻¹³	2.2 × 10 ⁴³
AXJ 1025+4714	156.4774, 47.2399	0.0	8.8	< –1.2	9.3 ^{+4.0} _{-2.5}	6.7 × 10 ⁻¹³	1.9 × 10 ⁴³
AXJ 1510+0742	227.6089, 7.6899	0.15	2.3	–1.1±0.3	13.9 ^{+10.6} _{-6.4}	1.0 × 10 ⁻¹³	1.8 × 10 ⁴⁴
AXJ 1951+5609	297.7547, 56.1647	7.0	3.9	1.4±0.2	0.63 ^{+1.09} _{-0.63}	1.2 × 10 ⁻¹³	7.2 × 10 ⁴⁴

* : The errors correspond to 1 σ .

†: A photon index of 1.7 is assumed. The errors correspond to 90% confidence level.

Table 3. Journal of optical spectroscopic observations.

Name	Telescope	Date	Integration time
AXJ 0223+4212	UH88	05 Oct. 2000	300 s
AXJ 0431–0526	UH88	06 Oct. 2000	600 s
AXJ 1025+4714	UH88	20 Mar. 2001	900 s
AXJ 1510+0742	UH88	21 Mar. 2001	900 s \times 3
AXJ 1951+5609	KPNO2.1m	20 Sep. 2000	900 s+1800 s \times 2

Table 4. Basic parameters of the sample.

Name	Redshift	m_R	M_V^*	Note
AXJ 0223+4212	0.0435 ± 0.0001	16.0	–21.1	Sb
AXJ 0431–0526	0.0596 ± 0.0002	15.6	–22.2	E/S0
AXJ 1025+4714	0.0617 ± 0.0001	16.9	–20.9	E/S0
AXJ 1510+0742	0.4595 ± 0.0001	20.1	–22.1	Extended
AXJ 1951+5609	0.9096 ± 0.0009	19.5	–24.2	...

*: $V - R = 0.22$ mag (power law index of -0.5) is assumed.

Table 5. Equivalent widths of narrow emission lines in units of \AA and their line-intensity ratios. [NII], [SII], and [OIII] denotes the [NII] λ 6583, [SII] λ 6716+6731, and [OIII] λ 5007 lines, respectively.

Name	H_α	[NII]	[SII]	[OIII]	H_β	$\log \frac{[\text{NII}]}{H_\alpha}$	$\log \frac{[\text{SII}]}{H_\alpha}$	$\log \frac{[\text{OIII}]}{H_\beta}$
AXJ 0223+4212	20 ± 1	20 ± 1	11 ± 2	< 5.7	5.9 ± 2.0	$0.00_{-0.04}^{+0.04}$	$-0.26_{-0.11}^{+0.10}$	< 0.16
AXJ 0431–0526	7.3 ± 0.4	7.4 ± 0.4	5.6 ± 0.6	5.8 ± 0.8	< 0.8	$0.00_{-0.04}^{+0.05}$	$-0.12_{-0.07}^{+0.07}$	> 0.80
AXJ 1025+4714	12 ± 1	5.8 ± 1.0	7.7 ± 1.1	8.4 ± 0.9	2.3 ± 0.8	$-0.31_{-0.12}^{+0.10}$	$-0.19_{-0.10}^{+0.09}$	$0.56_{-0.18}^{+0.23}$
AXJ 1510+0742	no data	no data	no data	69 ± 3	< 23	> 0.45

Table 6. Near-infrared magnitudes of our sample. The data of the first 3 sources are from 2MASS catalog, and the rest from our own observations. The number in parenthesis indicates a 1σ error.

Name	J	H	K_s	$J - K_s$
AXJ 0223+4212	14.53 (0.05)	13.74 (0.06)	13.35 (0.06)	1.18 (0.08)
AXJ 0431–0526	14.52 (0.04)	13.83 (0.05)	13.36 (0.05)	1.16 (0.06)
AXJ 1025+4714	15.12 (0.06)	14.49 (0.07)	13.94 (0.08)	1.18 (0.10)
AXJ 1510+0742	18.05 (0.05)	17.29 (0.07)	16.72 (0.05)	1.33 (0.07)
AXJ 1951+5609	18.22 (0.05)	18.03 (0.07)	16.98 (0.05)	1.24 (0.07)

Table 7. Summary of optical/X-ray properties of hard sources in the ALSS.

Name	z	m_R	f_X (2–10 keV) [erg cm ⁻² s ⁻¹]	$\log(f_X/f_R)$	E.W. [\AA]		Morphology
					H $_{\alpha}$	[OIII] λ 5007	
AXJ 131551+3237	0.128	18.1	2.6×10^{-13}	0.16	25 \pm 3	37 \pm 3	E/S0
AXJ 131501+3141	0.072	15.6	4.8×10^{-13}	-0.57	11 \pm 1	7 \pm 1	Early-type Spiral
AXJ 130926+2952	0.375	19.9	1.5×10^{-13}	0.64	no data	109 \pm 22	E/S0 or Early-type Spiral
AXJ 131210+3048	0.189	18.4	1.8×10^{-13}	0.11	13 \pm 2	16 \pm 2	E
AXJ 130840+2955	0.164	17.3	1.4×10^{-13}	-0.42	no data*	8.6 \pm 0.9	Spiral (Interacting?)

* : Not available due to atmospheric absorption.

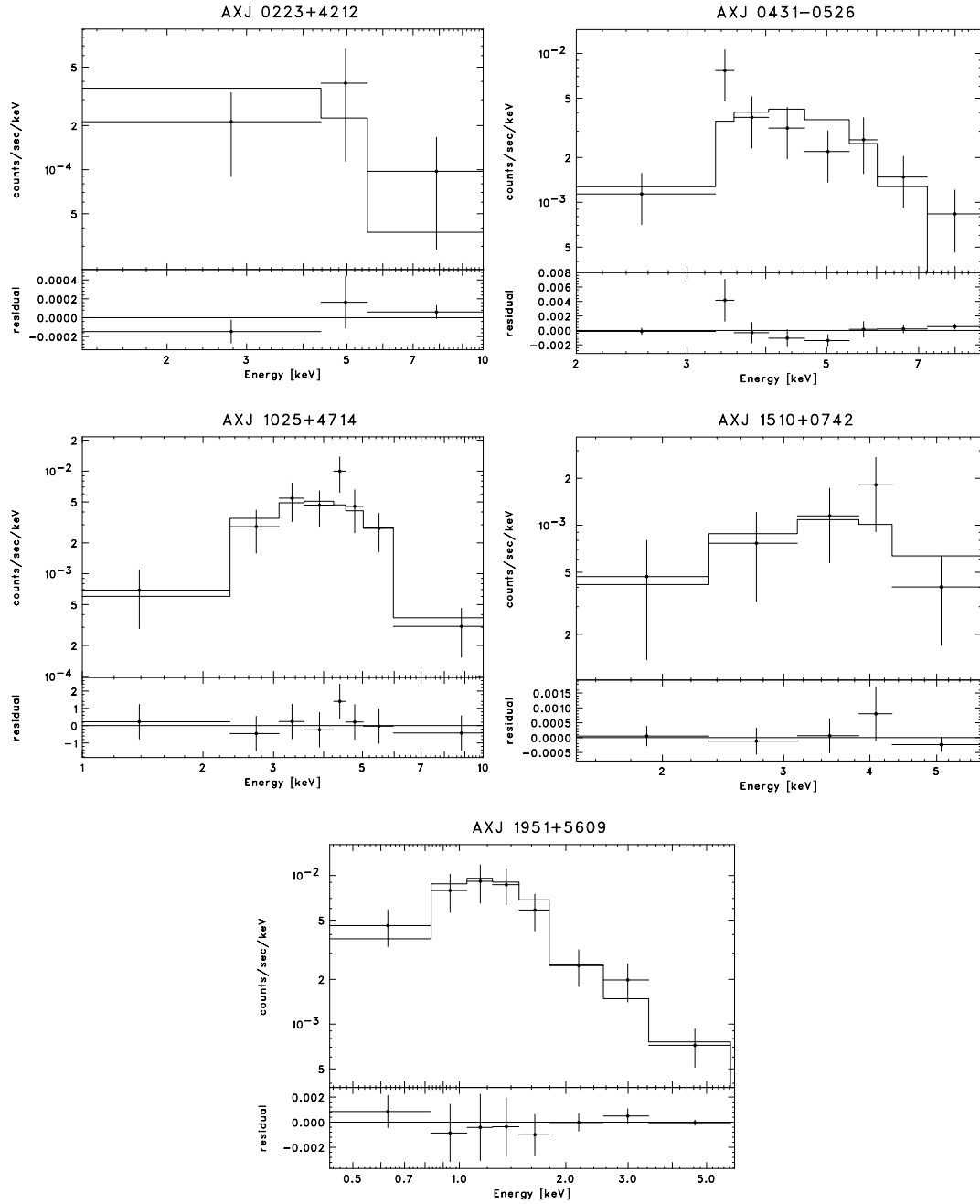


Fig. 1. The ACIS spectra of AXJ 0223+4212, AXJ 0431-0526, AXJ 1025+4714, AXJ 1510+0742, and AXJ 1951+5609, folded with the response. The best-fit model is an absorbed power law with a photon index of 1.7.

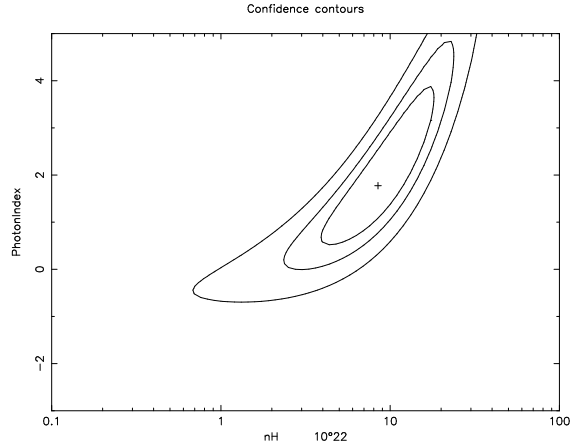


Fig. 2. The confidence contour of the photon index and the column density at the source redshift constrained from the ACIS spectrum of AXJ 1025+4714. Each contour represents 68 %, 90 % and 99 % confidence level.

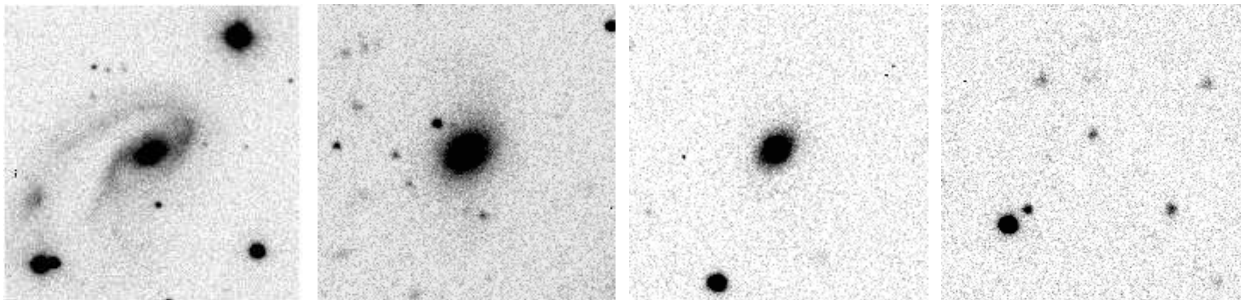
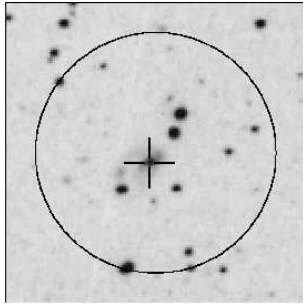
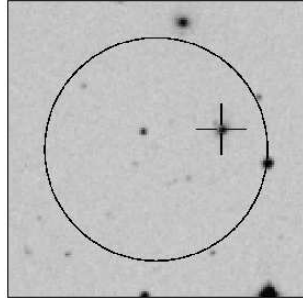
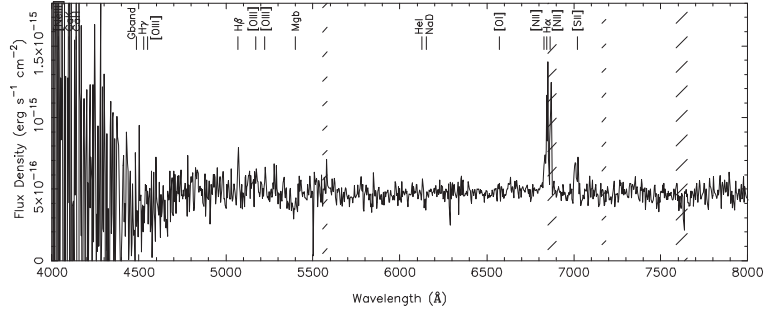


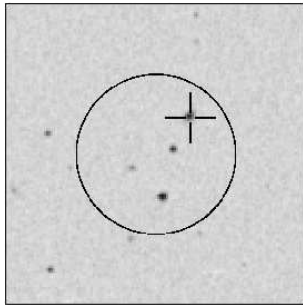
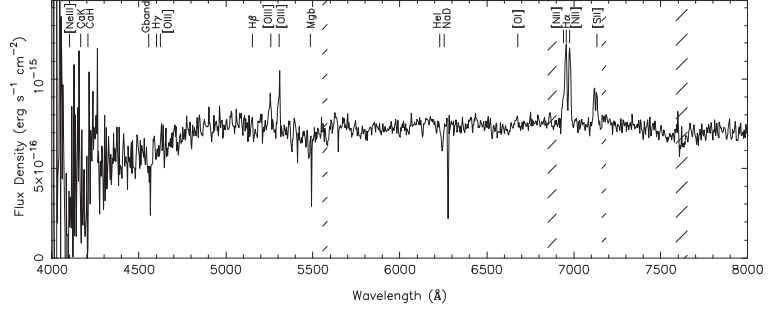
Fig. 3. No-filter 60 " \times 60 " images of AXJ 0223+4212, AXJ 0431-0526, AXJ 1025+4714, and AXJ 1951+5609 (from left to right).



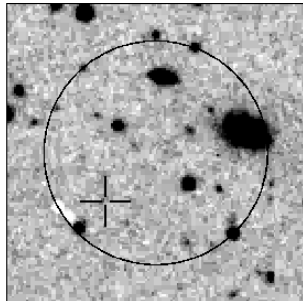
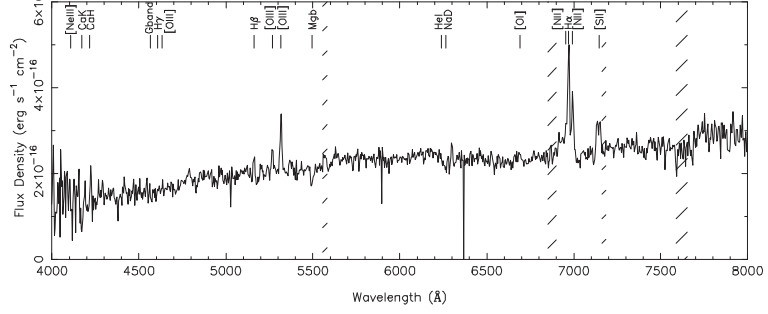
AXJ0223+4212:AGN:z=0.043



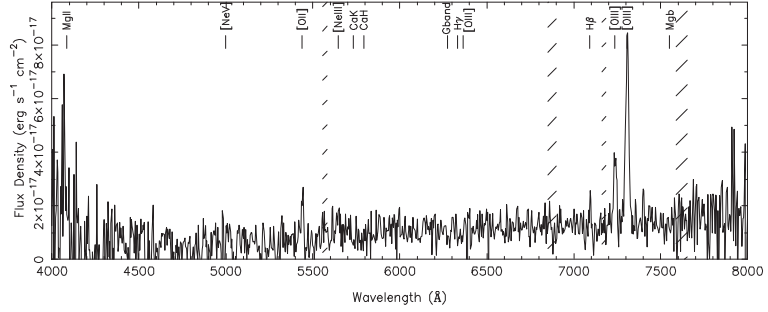
AXJ0431-0526:AGN:z=0.060



AXJ1025+4714:AGN:z=0.062



AXJ1510+0742:AGN:z=0.459



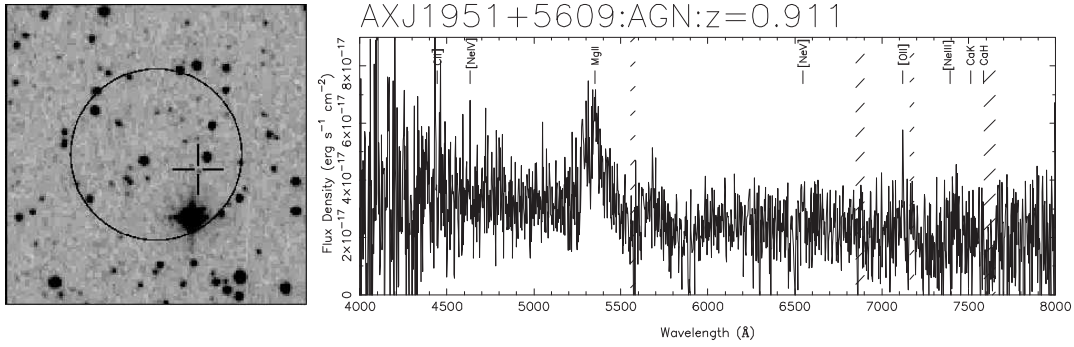


Fig. 4. Optical finding charts and spectra of identified objects. The finding charts are made from Digitized Palomar Observatory Sky Survey data. The field of view of the finding charts is $4' \times 4'$. The large circle corresponds to an error circle of ASCA, and the central position of the cross corresponds to the position of the Chandra source (with uncertainties of $1''$). In the spectra, the positions of principal lines are shown. The diagonal lines show the regions which are affected by absorption lines and emission lines of the atmosphere.

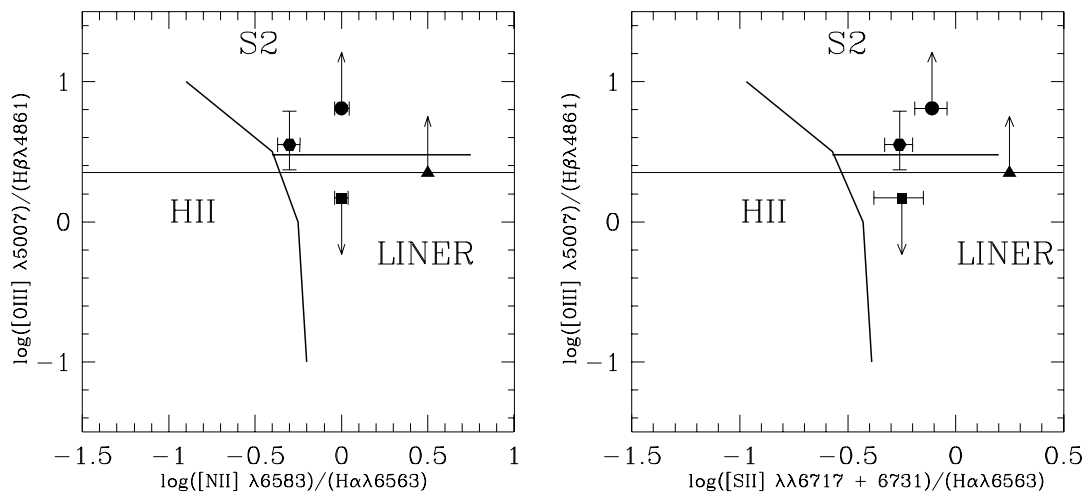


Fig. 5. The plot of intensity ratios of the optical narrow emission lines (filled square: AXJ 0223+4212, filled circle: AXJ 0431-0526, filled hexagon: AXJ 1025+4714, filled triangle: AXJ 1510+0742). Solid lines in the figure represent boundaries between Seyfert II galaxies, LINERs, and H II region-like galaxies, taken from Veilleux & Osterbrock (1987) and Veilleux (1995).

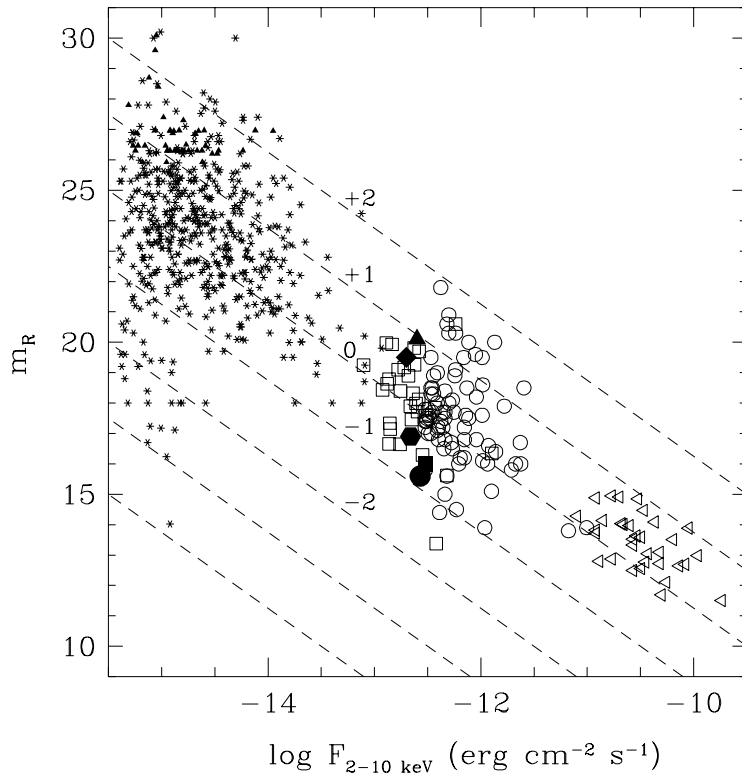


Fig. 6. Correlation between X-ray flux and optical magnitude (filled square: AXJ 0223+4212, filled circle: AXJ 0431–0526, filled hexagon: AXJ 1025+4714, filled triangle: AXJ 1510+0742, filled diamond: AXJ 1951+5609). Open triangles, open circles, and open squares are the AGNs from HEAO1 A2 (Piccinotti et al. 1982), the AMSS (Akiyama et al. 2002), the ALSS (Akiyama et al. 2000), respectively. Asterisks and crosses are the source from Chandra Deep Field North (Brandt et al. 2001, Barger et al. 2002), with crosses being upper limits on the optical magnitude. Dashed lines represent the X-ray to optical flux ratio of $\log f_X/f_R = +2, +1, 0, -1, -2, -3,$ and -4 from top to bottom.

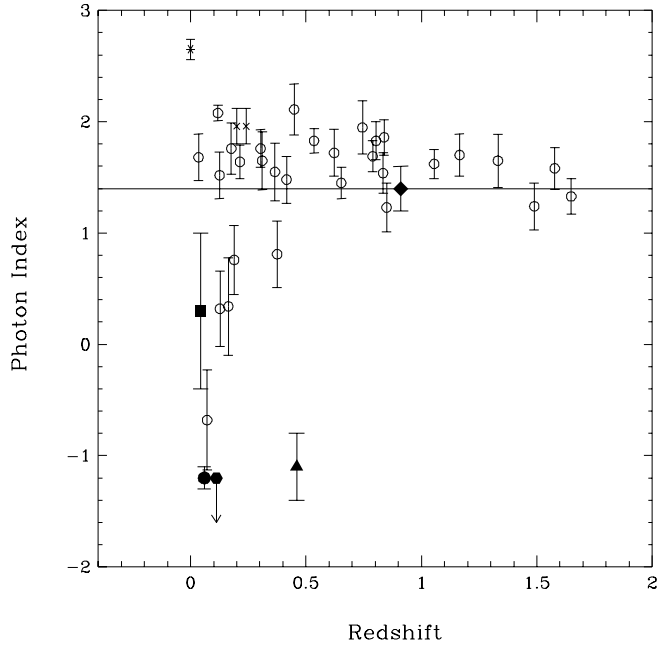


Fig. 7. The redshift versus an apparent photon index plot of our sample, (filled square: AXJ 0223+4212, filled circle: AXJ 0431–0526, filled hexagon: AXJ 1025+4714, filled triangle: AXJ 1510+0742, filled diamond: AXJ 1951+5609), compared with the ALSS sample (open circles: AGN, after Fig. 5 of Akiyama et al. (2000)).